Icarus 202 (2009) 147–159

Contents lists available at ScienceDirect

Icarus

www.elsevier.com/locate/icarus

Triaxial ellipsoid dimensions and poles of asteroids from AO observations at the Keck-II telescope

Jack Drummond [a,*], Julian Christou [b,1], Jerry Nelson [b]

[a] Starfire Optical Range, Directed Energy Directorate, Air Force Research Laboratory, Kirtland AFB, NM 87117-5776, United States
[b] University of California Observatories, Center for Adaptive Optics, University of California, Santa Cruz, CA 95064-1077, United States

ARTICLE INFO

Article history:
Received 8 May 2008
Revised 11 February 2009
Accepted 12 February 2009
Available online 26 February 2009

Keywords:
Asteroids
Adaptive optics

ABSTRACT

Five main belt asteroids, 2 Pallas, 129 Antigone, 409 Aspasia, 532 Herculina, and 704 Interamnia were imaged with the adaptive optics system on the 10 m Keck-II telescope in the near infrared on one night, August 16, 2006. The three axis dimensions and rotational poles were determined for Pallas, Antigone, Aspasia, and Interamnia, from their changing apparent sizes and shapes as measured with parametric blind deconvolution. The rotational pole found for Interamnia is much different from all previous work, including our own at Lick Observatory the previous month. Although images of Herculina were obtained at only two rotational phases, its rotation appears to be opposite to that predicted from the lightcurve inversion model of M. Kaasalainen, J. Torppa, and J. Piironen [2002. Icarus 159, 369–395]. A search for satellites was made in all of the asteroid images, with negative results, but three trailing stars around Herculina (200 km diameter), down to 8.9 magnitudes fainter and between 1 and 115 asteroid radii (100 to 11,500 km) from the asteroid, establishes an upper limit of 3.3 km for any object with the same albedo near Herculina.

Published by Elsevier Inc.

1. Introduction

A new era of ground-based study of asteroids has begun with resolved imaging through adaptive optics (AO) on large 8–10 m telescopes in the near infra-red, 1.2–1.6 μm (see Marchis et al., 2005, 2006, or Descamps et al., 2008, for some representative examples). Starting with asteroid 511 Davida (Conrad et al., 2006), not only can an asteroid's triaxial ellipsoid dimensions and rotational pole routinely be found in one or two nights with the method of Drummond (Drummond et al., 1985; Drummond, 2000), departures from the pure triaxial ellipsoid assumptions can be seen in such images, even before deconvolution processes are applied. The triaxial ellipsoid assumption provides a good fundamental reference, and then deeper studies of individual asteroids can be made by addressing observed departures from the assumptions. Ultimately, as for the case of 41 Daphne and its satellite (Conrad et al., 2008a), it is possible to measure the volume, mass, and thus density of an asteroid in one night (Merline et al., 2008; Conrad et al., 2008b), which for Daphne was the same night as the satellite's discovery. With deconvolution it is also possible to study albedo features, but the primary scope of our paper is to extract the triaxial ellipsoid parameters from a series of convolved images, without recourse to deconvolution, and is not to search for albedo variations on the face of the asteroid. Marchis et al. (2006) have also begun to observe asteroids with AO on large telescopes, and they should be consulted for comparable studies.

Having gained experience with observing binary stars (Christou and Drummond, 2006) and asteroids (Drummond and Christou, 2008) with the AO system behind the Shane 3 m telescope at Lick Observatory, we have made similar observations at the 10 m Keck-II telescope on one night in 2006. The results scale with the telescope size, and overall are three (or more) times better. We followed four asteroids, 2 Pallas, 129 Antigone, 409 Aspasia, and 704 Interamnia, as they rotated on the night of August 16, 2006, deriving their three axes dimensions and rotational poles under the assumption that they are smooth, featureless, bi- or triaxial ellipsoids rotating about their short axes. Two of the asteroids, Pallas and Interamnia, were observed at Lick Observatory (Drummond and Christou, 2008) a month before our Keck Observatory observations. Asteroid 532 Herculina was not placed well enough to image over a significant portion of its rotation, but we did make observations at two epochs to search for satellites.

Overall, in comparing the mean diameters of the four asteroids to IRAS results (Tedesco et al., 1992), the agreement is very good. For Pallas, Antigone, and Herculina, the lightcurve inversion (LCI) models[2] of Kaasalainen and colleagues (see Kaasalainen and

* Corresponding author.
[1] Currently at Gemini Observatory, Northern Operations Center, 670 N. A'ohoku Place, Hilo, HI, 96720.

[2] Available at http://astro.troja.mff.cuni.cz/projects/asteroids3D/web.php.

0019-1035/$ – see front matter Published by Elsevier Inc.
doi:10.1016/j.icarus.2009.02.011

Torppa, 2001; Kaasalainen et al., 2001) also stand in good agreement with our resolved images, either convolved or deconvolved. However, for Herculina we see an opposite rotation from that predicted with the LCI pole, and for Interamnia, we derive a pole that is quite different than others, including our own from Lick Observatory a month earlier.

Before addressing the asteroids individually, we broadly outline the principles involved in converting the apparent size, shape, and orientation of resolved asteroids to their triaxial ellipsoid dimensions and rotational pole, and show some of the reduction procedures.

2. Observations and reductions

On August 16, 2006, asteroids and check stars were observed with the NIRC-2 camera behind the Keck-II 10 m telescope and adaptive optics, and through the K_s filter having a central wavelength of $\lambda = 2.146$ µm and a bandwidth of 0.311 µm. Observations were obtained in a five-spot pattern, where five co-added one second exposures are made in the middle of the frame and four other sets are made near the middle of each of the four quadrants. At $0.010''$/pix, the field of view of the 1024×1024 pixel camera is about 10 arc seconds, and the location of the observations in the five-spot pattern are approximately at 2.5, 5, or $7.5''$ in the field. A sky was formed by taking the median of the five frames, and then subtracted from each exposure.

From 17 observations (5 exposures each) of check stars throughout the night, with exposure times of either 0.18 or 0.25 s, the average Strehl was found to be 0.57 ± 0.04. However, we do not use these check stars in our reductions because we assume an analytic function for the point spread function (PSF). Previously, with smaller telescopes, we have assumed that the PSF for the asteroid observations is Lorentzian (Drummond, 1998) in shape, and fit the convolved images in the frequency domain, where a smooth featureless triaxial ellipsoid asteroid can be modeled with a Bessel function of the first kind of order one, $2J_1(\vec{x})/\vec{x}$ where $\vec{x}$ is a Fourier plane position vector, and the Lorentzian PSF can be modeled as a modified Bessel function of the second kind of order zero, $K_0(\vec{x})$, and where the convolution becomes a product of these two functions. However, for AO observations at the Keck 10 telescope where the PSF is oversampled, we have found that the best analytic representation of the PSF is the sum of a Lorentzian and the Airy pattern appropriate for the size of the telescope. Allowing both the Lorentzian and Airy to vary in fits of the check stars shows that the Airy remains close to its expected size while the Lorentzian varies in size and relative contribution. From 85 images of check stars, the Airy radius was found to be 2.22 ± 0.14 pixels, compared to a theoretical 2.23 pixels, and the relative contribution of the Airy to the total PSF as expressed by the ratio of peak intensities in the image domain was $I_A/(I_L + I_A) = 0.79 \pm 0.09$.

In poor AO performance conditions, when the Strehl is low, the PSF becomes very Lorentzian in appearance, but even as the Strehl gets higher, as in our case, a Lorentzian model still suffices for least squares fitting for asteroid parameters. As proof, we performed two fits each of two of the asteroids, Pallas and Antigone, one using a Lorentzian model PSF and one using a combination fixed Airy plus variable Lorentzian model, and for both asteroids the measured sizes differed by no more than one km between the two fits. Therefore, for this current data set, we have continued the tradition of using a Lorentzian-only PSF model to derive the asteroid parameters.

This method of simultaneously obtaining both asteroid and PSF parameters from the observation without recourse to separate PSF measurements is called Parametric Blind Deconvolution or PBD (Drummond, 1998, 2000). Another reason that the fit is made in the Fourier domain is because in the image domain hard-edged objects represent discontinuities which are not amenable to least squares fitting.

Fig. 1 illustrates the sequence of data reduction. For each of the four of the asteroids studied in full below, Fig. 1 shows a single sample image and its corresponding FFT. In the frequency or Fourier domain, the asteroid sizes and orientations are determined by the number and locations of the minima in the FFT, which are not greatly affected by the actual shape of the PSF. The Fourier fits to the sample images are also shown in Fig. 1 (third column), and inverse Fourier transforming the fits yields the convolved images in the fourth column to compare to the actual images. However, once the fit in the Fourier plane is made, we can clean the image of the PSF by dividing the FFT of the image by the FFT of the Lorentzian found in the fit, and then inverse FFT the quotient. As expected, these simple linear deconvolutions do not show surface details, and are not displayed here for Pallas or Aspasia. However, they are shown for Antigone, Herculina, and Interamnia. Because it is so elongated, a sequence of simple linearly deconvolved images nicely shows Antigone rotating, and linearly deconvolved images of Herculina and Interamnia are used to illustrate discrepancies in their rotational pole locations. A more sophisticated iterative deconvolution algorithm such as performed by Marchis et al. (2006), or by Carry et al. (2008, 2009) for both 1 Ceres and 2 Pallas with MISTRAL, might show surface detail, but such analysis is beyond the scope of this paper because we are interested primarily in extracting triaxial ellipsoid parameters from the AO images.

3. Triaxial ellipsoid results

Table 1 contains ephemeris information for the asteroids on August 16, 2006, gathered with JPL's Horizons service. The 2000 coordinates of each asteroid are listed, along with its rotational period, and V magnitude. NtS is the position angle of the Sun, measured east from north, looking at the asteroid, and ω is the solar phase angle. The Earth and Sun distance are listed next, and the final column of Table 1 is the scale at the distance of the asteroid.

After taking the FFT of an image, in the Fourier domain we fit for nine parameters, six for the asteroid (an amplitude, apparent long (α) and short (β) dimensions, an orientation angle (pa), and x and y centers), and three for the Lorentzian PSF (long and short dimensions and an orientation angle). Compiling the asteroid's apparent size and orientations as a function of rotational phase ψ, with another least squares fit program we then find the six triaxial ellipsoid parameters, three dimensions and three angles, given in Table 2. In addition to the three diameters, θ, the asterocentric sub-Earth latitude is listed for each asteroid on this night. The position angle of the line of nodes, which is the intersection of the asteroid's equator with the plane of the sky measured eastward from celestial north, is N. The direction to the asteroid's north pole (defined with the right hand rule) is $N + 90°$. And finally, ψ_0 is the instant of maximum projected area, or when the maximum equatorial diameter, a, is seen unprojected in the plane of the sky. Given the position of the asteroid, we calculate the location of each asteroid's pole with N and θ, and give both celestial and Ecliptic coordinates in Table 3.

Uncertainties for the parameters are a direct product of the non-linear least squares program used to turn the apparent ellipses into a single triaxial ellipsoid. They are determined from the residuals to the fit, and as such, they reflect both measurement or observational scatter and departures from the model assumption (a smooth, featureless, triaxial ellipsoid rotating about its short axis). In other words, they are one standard deviation precisions of the parameters based on the fit of the observations to the model. Any uncertainties due a uniform systematic effect is not part of the least squares fitting uncertainties. Comparing

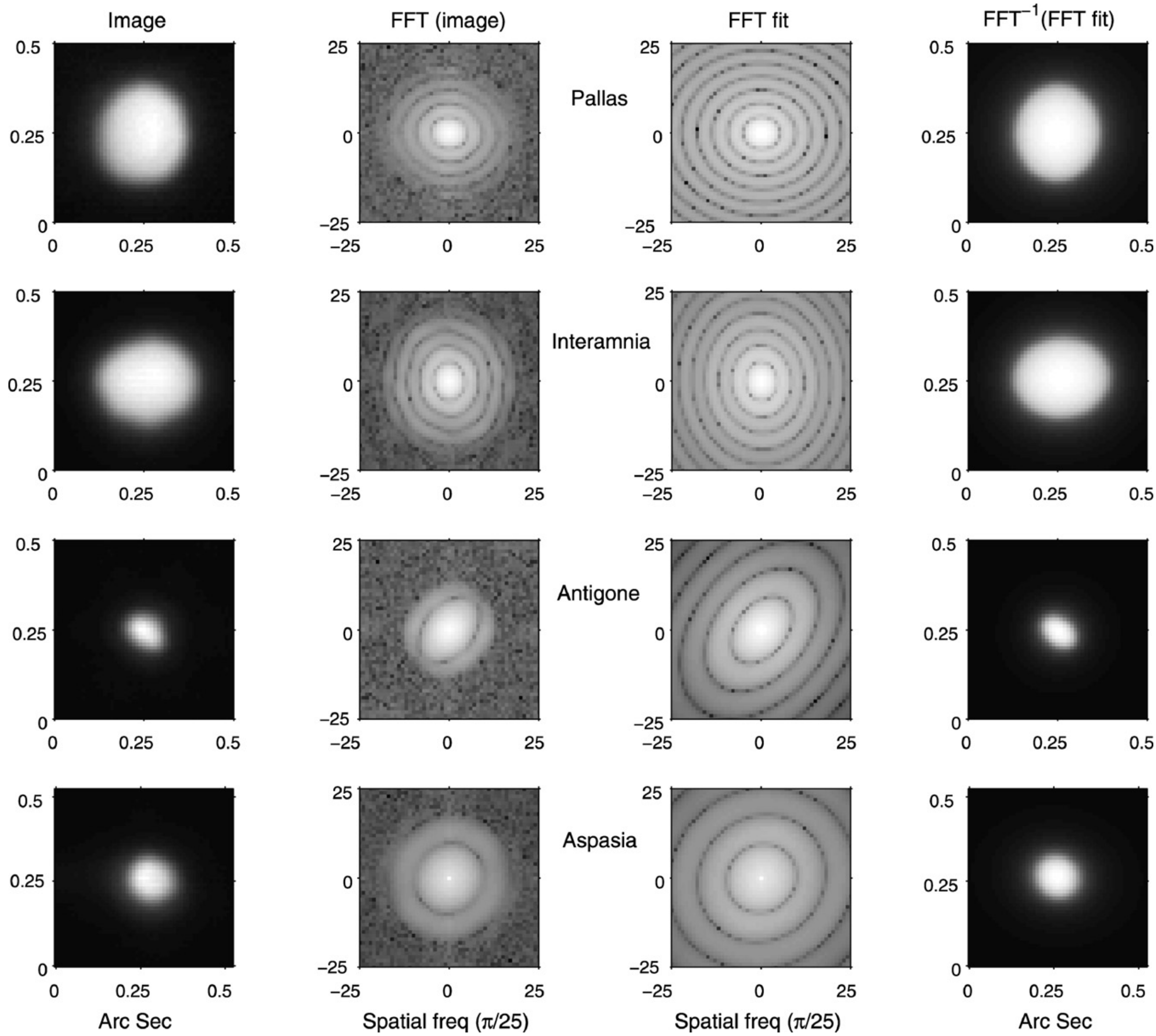

Fig. 1. Sample images of asteroids, their Fourier transforms, and least squares fits. A single image of each of the asteroids is shown in the left column, and the Fourier transform of the images are shown in the second column. To show subtle but important detail, the absolute values of the FFT's are displayed on a log scale. Notice how the high frequency cutoffs are well demarcated in all of the FFT's, outside of which appears only noise. Also notice how the large asteroids Pallas and Interamnia show several ripples or minima while the smaller asteroids show only one or two. The third column shows the fit to the second column, where the fit is for the product of the asteroid and PSF in the Fourier domain. The fits are performed interior to the high frequency noise, but the entire model is shown. Inverse Fourier transforming these fits produces the images from the fits shown in the fourth column.

Table 1
August 16, 2006 asteroid observing log (J2000).

Asteroid	RA (°)	Dec (°)	Per (h)	V	NtS (°)	ω (°)	$r_\oplus$ (AU)	$r_\odot$ (AU)	km/mas
2 Pallas	270.8	+17.2	7.813	9.9	296.3	15.5	2.758	3.350	2.000
129 Antigone	8.0	−7.3	4.957	11.5	77.6	13.4	2.090	2.922	1.516
409 Aspasia	7.6	+18.8	9.020	11.6	54.8	17.6	1.923	2.663	1.395
532 Herculina	258.5	−19.7	9.405	10.5	276.1	19.6	2.117	2.716	1.535
704 Interamnia	328.1	+9.3	8.727	10.3	5.9	8.5	1.746	2.707	1.266

Table 2
Asteroid ellipsoid parameter results.

Name	a (km)	b (km)	c (km)	θ (°)	N (°)	ψ_0 (UT)
2 Pallas	548 ± 3	504 ± 3	459 ± 14	+41 ± 6	2 ± 1	4.89 ± 0.06
129 Antigone	163 ± 4	133 ± 2	90 ± 28	+46 ± 10	231 ± 3	10.25 ± 0.06
409 Aspasia	198 ± 5	172 ± 3	172 ± 3	−34 ± 3	293 ± 5	10.01 ± 0.12
704 Interamnia	349 ± 4	339 ± 3	274 ± 22	−26 ± 16	275 ± 1	6.62 ± 0.19

Table 3
Asteroid ellipsoid poles (J2000).

Name	Eq		Pole	Ecl	
	RA (°)	Dec (°)	Err Rad (°)	λ (°)	β (°)
2 Pallas	41	−13	3	34	−27
129 Antigone	222	+39	5	202	+52
409 Aspasia	58	+65	4	72	+43
704 Interamnia	343	+73	3	47	+66

the sizes of seven of our images of Pallas as derived from our method of fitting the images in the Fourier domain, to the contours of MISTRAL deconvolved images produced by Carry et al. (2009), we find that the contours in the image domain are systematically greater than our sizes in the frequency domain by 2.0 ± 1.3%. This is either due to the PSF not being fully deconvolved from the images with MISTRAL, or the size of the PSF being overestimated with

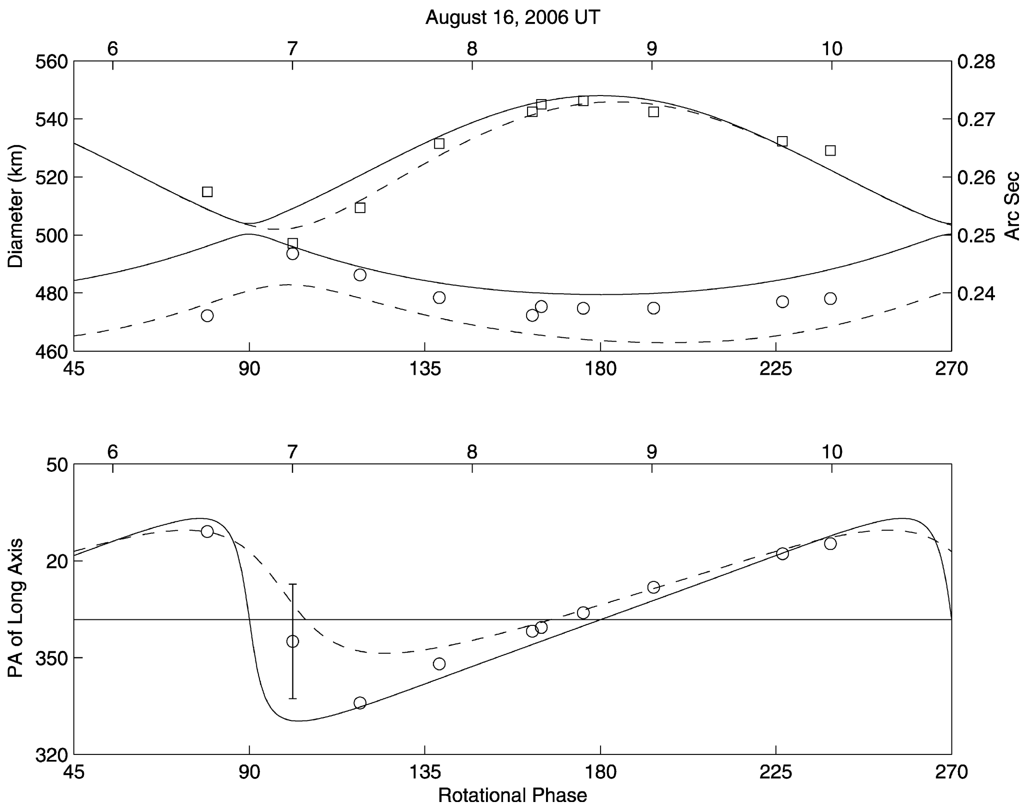

Fig. 2. Triaxial ellipsoid fit for Pallas. In the upper sub-plot, the squares and circles denote the measured major and minor axes ellipse diameters, and in the lower sub-plot, the circles show the measured position angle of the long axis. The solid line is the triaxial ellipsoid fit, and the dashed line is the terminator ellipse for the fit. Except for the one observation in the bottom sub-plot when the position angle was virtually indeterminate because the asteroid was nearly circular in appearance, the uncertainties for all of the measurements are about the size of the symbols.

Table 4
Volumes and mean diameters.

Name	Volume (km^3)	$\bar{d}$ (km)	IRAS d (km)
2 Pallas	$6.64(\pm 0.21) \times 10^7$	502 ± 5	498 ± 19
129 Antigone	$1.02(\pm 0.32) \times 10^6$	125 ± 13	124[a]
409 Aspasia	$3.05(\pm 0.11) \times 10^6$	180 ± 2	162 ± 7
704 Interamnia	$1.70(\pm 0.14) \times 10^7$	319 ± 9	317 ± 5

[a] Not observed by IRAS; diameter is from the IMPS ground-based catalog (Tedesco et al., 1992).

our Fourier fitting. At any rate, this suggests that there may be an additional systematic uncertainty of 1–2% not reflected in the uncertainties in Tables 2–4.

Of interest might be the mean diameters of these asteroids, and the corresponding volumes. For convenience, Table 4 gives these quantities, where $\bar{d} = (abc)^{1/3}$. For comparison the IRAS diameters are also given, although they are actually from the mean of projected areas at random rotational phases over limited ranges of asterocentric latitudes, and do not necessarily represent the mean of all three true axes dimensions.

3.1. Individual asteroids

We now discuss each asteroid individually. For each asteroid, except Herculina, a two sub-plot triaxial fit figure is shown with an ordinate range of 100 km in the upper sub-plot and an abscissa range of a full period rotation of 360°, except Pallas' abscissa which only ranges over 135°. For the position angle in the lower sub-plot, the ordinate range is 180° for Antigone and Aspasia which appear to rotate through 360°, 90° for Pallas which rocks about its line of nodes, and 30° for Interamnia which merely nods about its line of nodes.

Inheriting the lists from Magnusson (1989), Kryszczyńska et al. (2007) now maintain a web site[3] with the various poles and axial ratios derived from lightcurves and other techniques for all asteroids. In the following sections, each of our asteroids, except for Herculina, has displayed on an Ecliptic globe the locations of all poles from this web site for J2000. In the text poles are generally listed as Ecliptic coordinates [λ; β], both in degrees.

3.1.1. 2 Pallas

Pallas was favorably placed during the summer of 2006 and we obtain the results listed in Tables 2–4, and shown in Figs. 2 and 3. Even though Pallas only moved 6° between our observations at Lick Observatory on July 18 (Drummond and Christou, 2008) and at Keck Observatory on August 16, this was sufficient to break the normal two-fold ambiguity in poles with our method, as shown in Fig. 3.

Pallas has been studied many times, and many estimates of its pole have been made, although the ambiguity inherent in most techniques has not been satisfactorily resolved. Kryszczyńska (footnote 3) finds a consensus pole for Pallas at Ecliptic coordinates [λ; β] = [44; −9], and axial ratios of $a/b = 1.1$ and $b/c = 1.05$. From our dimensions in Table 2 we obtain $a/b = 1.09 \pm 0.01$ and $b/c = 1.10 \pm 0.04$, in good agreement, while our favored pole is located at [34; −27], some 20° away.

Comparing the uncertainties for the pole and the dimensions obtained with the Lick Observatory 3 m telescope and the Keck Observatory 10 m telescope clearly illustrates the advantage to the larger aperture. From Lick Observatory we found the uncertainties on Pallas' dimensions to be 17 × 15 × 128 km, while from Keck

[3] http://vesta.astro.amu.edu.pl/Science/Asteroids/.

Observatory we found uncertainties of $3 \times 3 \times 15$ km, or 5 times better for a and b, and even more for c. The ratio of the uncertainty areas around the poles, $(1 - \cos 6.3°)/(1 - \cos 2.7°) = 5$, also indicates a location 5 times better determined from Keck Observatory.

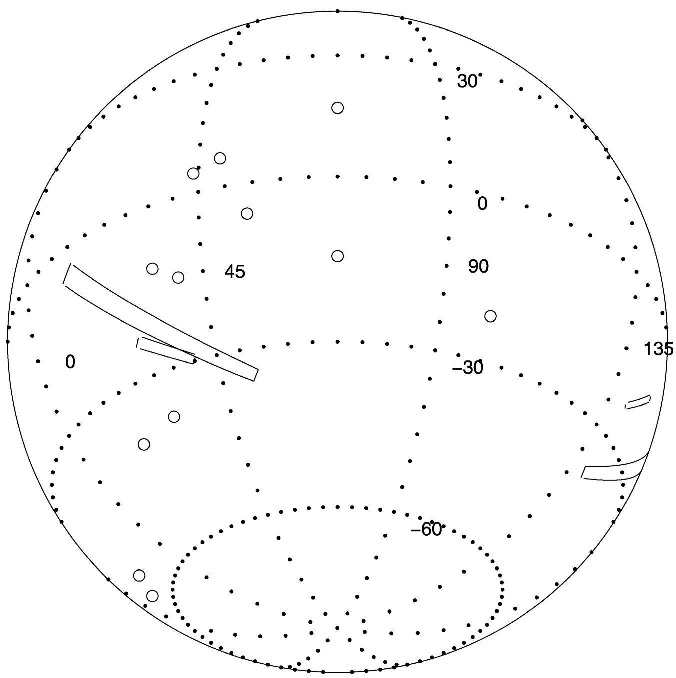

Fig. 3. Rotational poles for Pallas on an Ecliptic globe. Previous determinations of Pallas' poles are indicated by small circles, and our two possible poles are at the center of the small wedges, which denote the region of uncertainty. The large wedges are from our observations at Lick Observatory a month earlier, and the two-fold ambiguity for the location of the pole is broken in favor of the region where the large and small wedges are closest. The radius of a circle having the same area as the uncertainty wedge is used for the pole error in Table 3.

For a detailed picture of Pallas, we defer to Carry et al. (2009), who include our images in an extensive evaluation of its appearance from the Very Large Telescope 8 m and Keck 10 m telescopes between 2003 and 2007.

Table 5 gives the size and orientation of Pallas derived from two well observed occultations (Wasserman et al., 1979; Dunham et al., 1990) taken from the NASA's Planetary Data System's web site[4] (Dunham and Herald, 2008). They are plotted in Figs. 4 and 5 at rotational phases according to the model of Table 2 and the latest sidereal period of 0.3255512 days from the lightcurve inversion web site (footnote 2).

The outlines, especially the minor axes dimensions, are larger than our model predicts. Simply scaling our triaxial ellipsoid does not satisfactorily reduce the differences, and neither does varying any of the individual axis dimensions from AO images, nor does applying limb darkening corrections to our data. Nothing we can do to our data will lead to a good prediction for the occultation results for Pallas.

[4] http://www.psi.edu/pds/resource/occ.

Table 5
Pallas occultation results.

Date	RA (°)	Dec (°)	α (km)	β (km)	pa_α (°)
May 29, 1978 5.0674 UT	259.9	+25.4	553.5 ± 1.6	528.4 ± 3.8	321.0 ± 6.6
May 29, 1983 4.4704 UT	289.1	+21.4	528.6 ± 1.0	512.3 ± 2.7	328.3 ± 4.3
E–W dim/1.1					
May 29, 1978			546.0	487.0	348.3
May 29, 1983			525.0	468.9	352.8

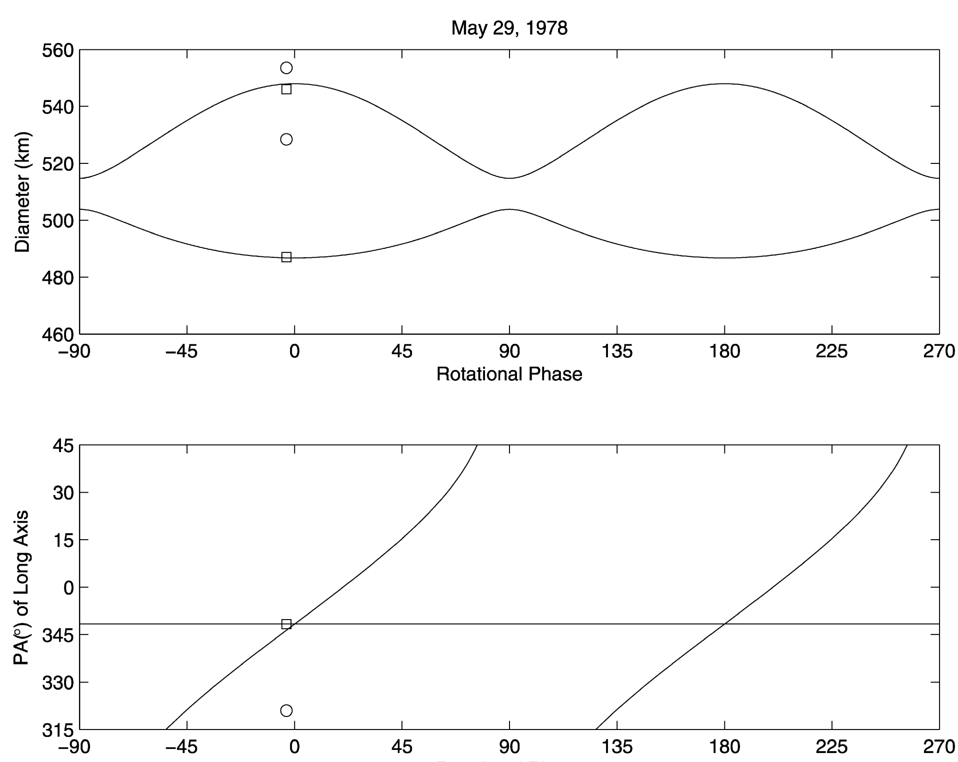

Fig. 4. Pallas's occultation size and orientation (Table 5) at the Table 2 AO model predicted rotational phases in 1978. The actual measurements are circles, and the lines show the predicted parameters over a rotation. The squares are the parameters if the east–west dimensions for the occultations are divided by 1.1, and then they fall almost exactly where predicted.

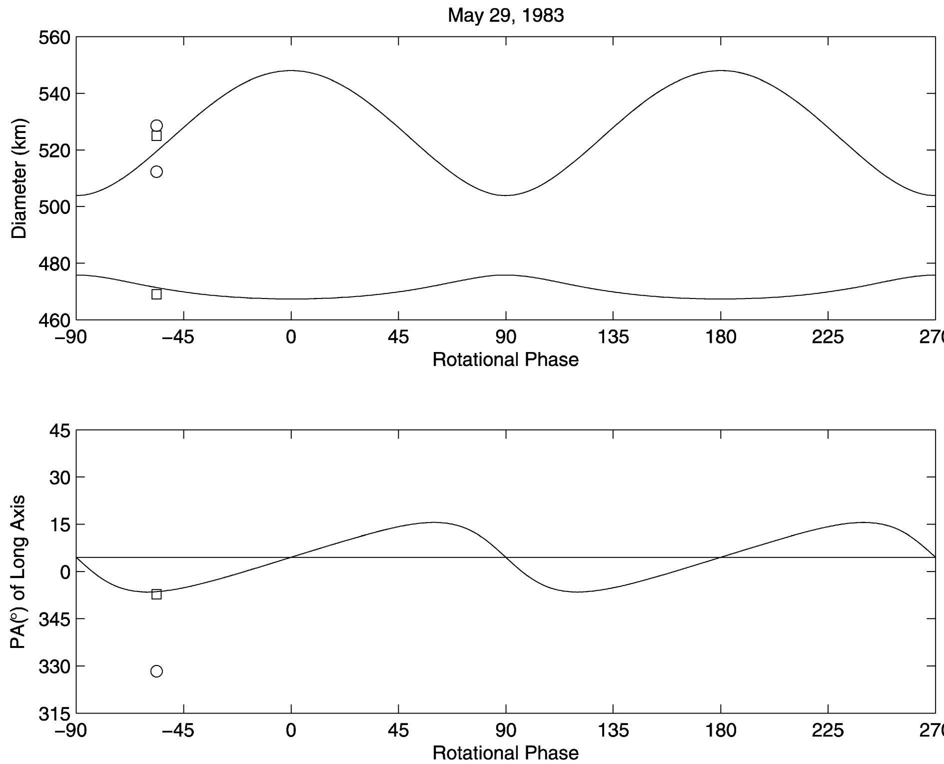

Fig. 5. Same as previous figure, but for the 1983 Pallas occultation.

Table 6
Pallas occultation residuals (observed minus predicted).

Date	$\Delta\alpha$ (km)	$\Delta\beta$ (km)	Δpa_α (°)
1978	2.8	20.8	−25.2
1983	4.6	20.4	−25.3
E–W dim/1.1			
1978	−1.0	0.1	1.9
1983	2.8	−1.2	−0.8

However, if the east–west occultation dimensions are reduced by 10%, then a nearly exact match occurs between our model and the occultations. In other words, if each reported occultation ellipse is squeezed towards the center in the east–west line, and then refit for a new ellipse, the new ellipse parameters as reported in Table 5 satisfy the triaxial ellipsoid solution of Table 2. A comparison of the residuals is given in Table 6, and a comparison of the predicted 1978 and 1983 appearances of the 2006 model to the observed ellipses (dotted lines) is shown in Fig. 6. When the adjusted ellipses are over-plotted, they are indistinguishable from the edge of the models. However, it is probably merely a coincidence that both occultations are off from our model in exactly the same way, and at this point the discrepancies remain unexplained. Future comparisons of occultation and AO results may shed some light on systematics that may be at play with either technique.

3.1.2. 129 Antigone

Although Antigone was well observed over 225° of rotation, because the sub-Earth latitude was so high, +42°, its c dimension, as given in Table 2, was only poorly constrained. Adaptive optics observations at a lower latitude will provide a less fore-shortened view of c with a concomitant improvement in its uncertainty. The triaxial ellipsoid fit is shown in Fig. 7. Because it is a bright, rapidly rotating asteroid, Antigone has been studied often and has many pole determinations as shown in Fig. 8. The ambiguity between our two poles is clearly resolved by merely inspecting the figure.

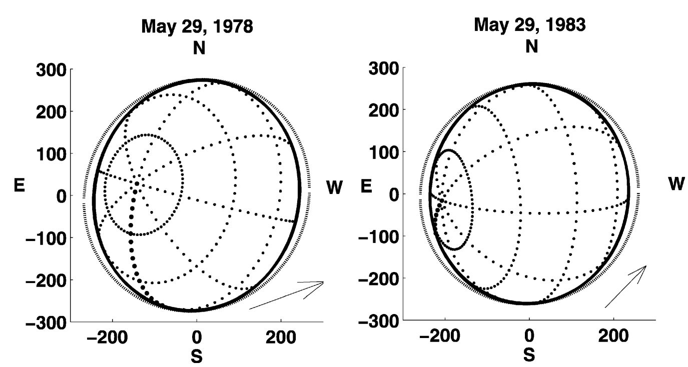

Fig. 6. The triaxial ellipsoid model prediction for the instances of the 1978 and 1983 occultations of Pallas. The observed ellipses are drawn with dotted lines encompassing the model globes. The adjusted observed ellipses, adjusted by squeezing the dotted ellipses by 10% in the east–west directions, are also drawn but are indistinguishable from the edges of the globes. The arrows at lower right depict the relative velocities (31″/h in 1978 and 22″/h in 1983) and directions of motion of the asteroid with respect to the occulted star.

The mean of eight determinations of axial ratios as listed by Kryszczyńska (footnote 4) is $a/b = 1.32 \pm 0.07$ and $b/c = 1.03 \pm 0.03$. We find $a/b = 1.22 \pm 0.04$, in fair agreement, but our $b/c = 1.48 \pm 0.46$ begs for observations at a lower sub-Earth latitude. However, the strong curvature for the minor axes dimensions in Fig. 7, out of phase with the major axes dimensions, argues against a b/c near unity. For a $b/c = 1$, the lower curve of the upper subplot would be straight.

Our linear deconvolutions are shown in Fig. 9. Torppa et al. (2003) have produced a model of Antigone by inverting lightcurves (footnote 2). Using their pole at $[\lambda; \beta] = [207; +58]$ (plotted in Fig. 8) and sidereal period of 4.957154 h, we can extrapolate their model from their initial epoch on May 29, 1971 to the time of our observations. Fig. 9 then compares our deconvolved images to their model at the same rotational phase. In particular, the pointed end

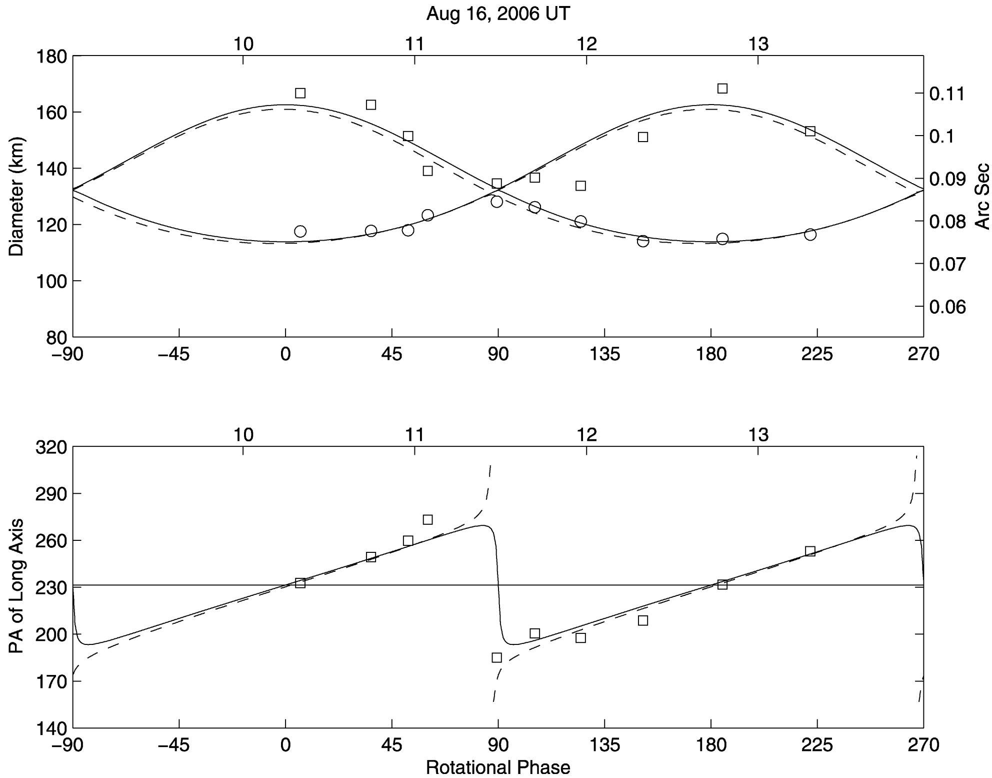

Fig. 7. Same as Fig. 2, but triaxial ellipsoid fit for Antigone.

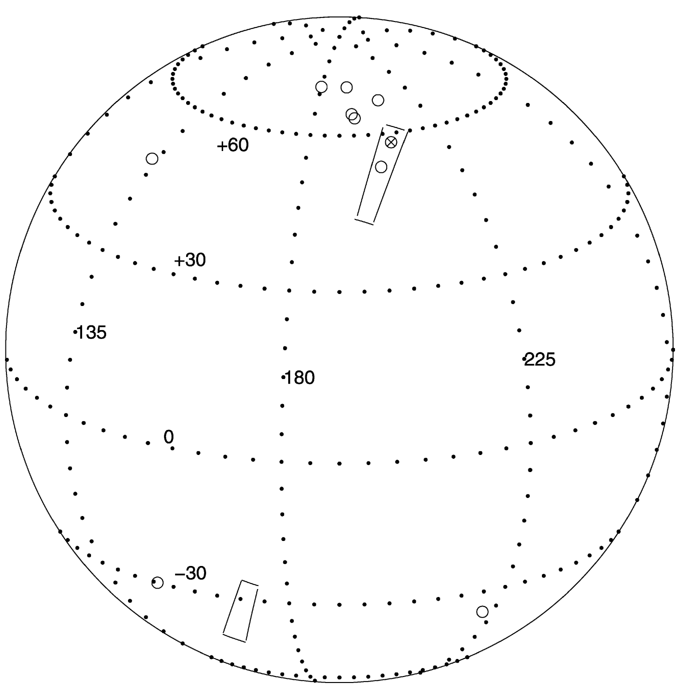

Fig. 8. Rotational poles for Antigone on an Ecliptic globe. The circled x marks the pole of Torppa et al. (2003), which is used to generate the lightcurve inversion model displayed in Fig. 9.

that leads to the measured apparent major axis being longer than the ellipsoid fit at $\psi = 180°$ in Fig. 7 is visible in both the model and the images in frames 8 and 9.

3.1.3. 409 Aspasia

Fitting the five observations of Aspasia for a triaxial ellipsoid revealed a c dimension a little greater than b. Therefore, we adopt a prolate spheroid assumption of $b = c$, reducing the number of unknowns from 6 to 5. We give the biaxial ellipsoid results in Tables 2–4, we show the fit in Fig. 10 and the pole locations in Fig. 11. The 17.6° solar phase angle creates the unusual curves in Fig. 10, where the dashed lines indicate the size and orientation of the terminator ellipse at each rotational phase. The measured apparent ellipses should be between the terminator parameters and the asteroid projected ellipse parameters, indicated by the solid lines. The long axis dimension from the last observation appears to be a major departure from the fit, and could be indicative of a topographic feature on the asteroid.

There has only been one effort to locate Aspasia's rotational pole from lightcurves. Using the amplitude-magnitude method, Blanco and Riccioli (1998) found four possible regions, a prograde and a retrograde spin each for two axes. While our method produces a two-fold ambiguity, together, because the ambiguities are different, the ambiguities are broken in favor of the northern pole as shown in Fig. 11. Blanco and Riccioli find axial ratios of $a/b = 1.137$ and $b/c = 1.080$, in good agreement with our $a/b = 1.13 \pm 0.03$ and $b/c = 1.00 \pm 0.02$.

3.1.4. 532 Herculina

Only two sets of five-spot observations (5 co-added 1 s exposures per spot) were made of Herculina separated by 20 min or 14° of rotation. This is not enough rotational coverage to determine the asteroid's pole or shape with any confidence, but after fitting the images for the asteroid and PSF parameters, the correct trend for an ellipsoid of increasing α and decreasing β is observed (Table 7). Furthermore, a biaxial fit can be made on images obtained at two epochs, although then the small axis length never changes by definition. The two possible poles from biaxial ellipsoid fits both yield high northern sub-Earth latitudes of $\theta = +62°$ or $+44°$, which produce counterclockwise rotation during our observations.

The lightcurve inversion model (footnote 2) of Kaasalainen et al. (2002), with a pole at $[\lambda; \beta] = [288; +11]$ and a sidereal pe-

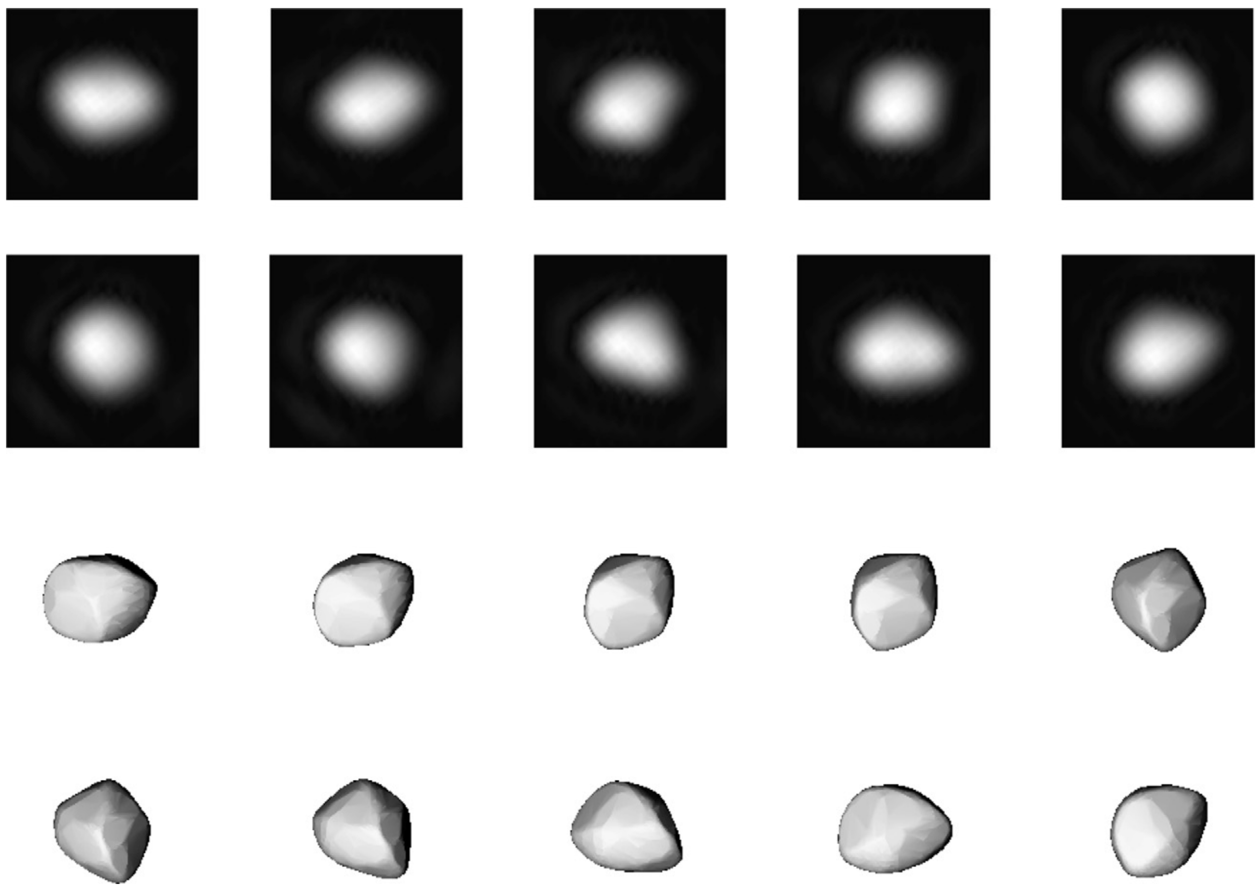

Fig. 9. Comparison of deconvolved images of Antigone to the lightcurve inversion model of Torppa et al. (2003).

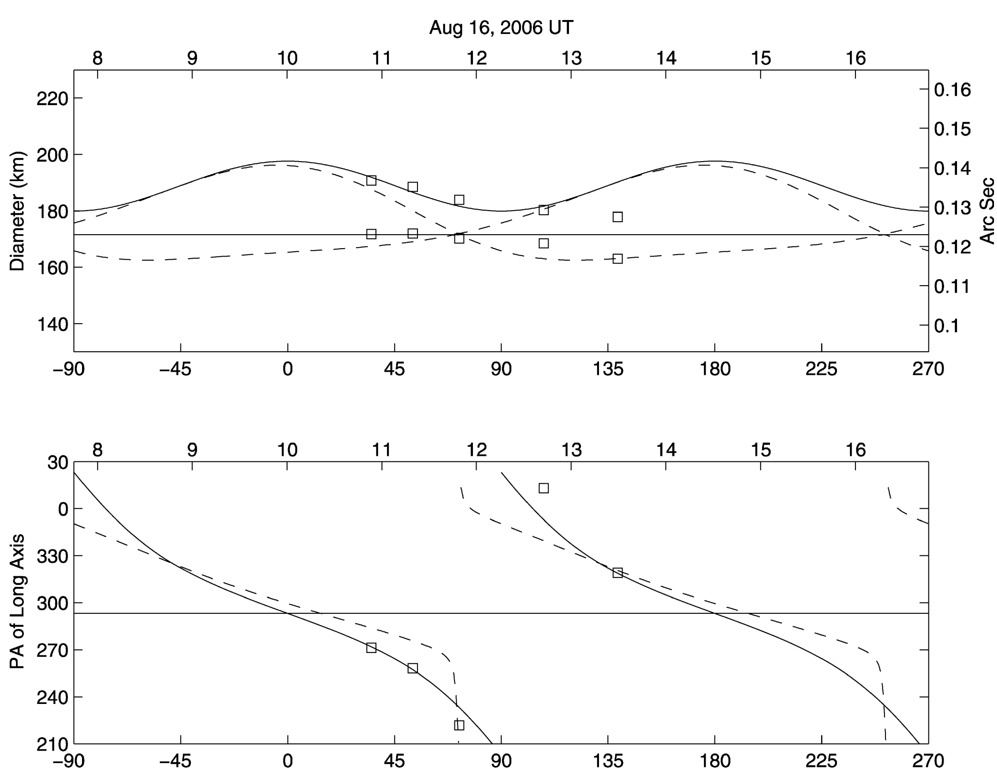

Fig. 10. Northern pole, biaxial ellipsoid fit for Aspasia. The unusual shape to the dashed lines in the top sub-plot, corresponding to the terminator ellipse, is caused by the moderate solar phase angle of 17.6° on a biaxial ellipsoid. Both the projected ellipse and the terminator ellipse will rotate through 360°, but at different varying rates. This leads to the unusual curve in the top sub-plot.

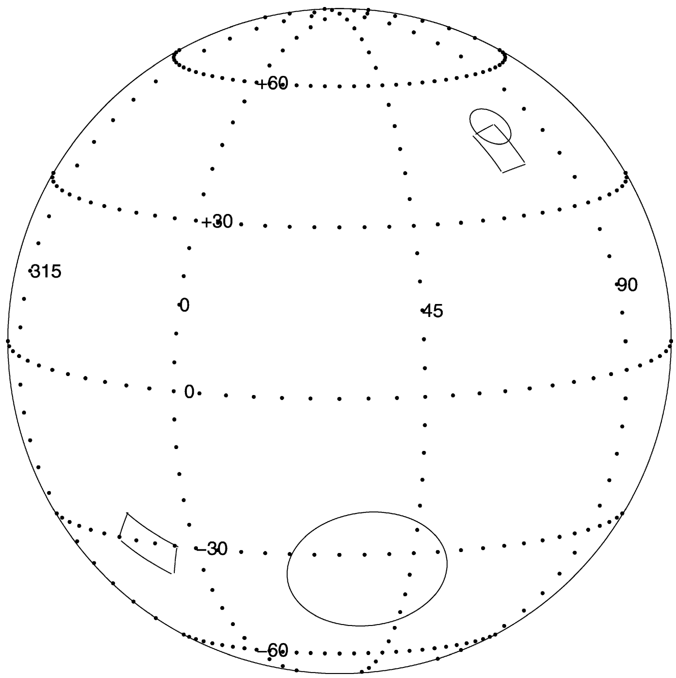

Fig. 11. Rotational poles for Aspasia on an Ecliptic globe. Our two possible poles are the wedges (denoting the regions of uncertainty) in each hemisphere, and the circles (also denoting regions of uncertainty) are two poles are from Blanco and Riccioli (1998). Since the two northern hemisphere poles are closer than the two in the southern hemisphere, the northern region is adopted for the pole. The amplitude–magnitude method of Blanco and Riccioli produces two additional poles, but on the other side of the Ecliptic globe.

Table 7
532 Herculina apparent size and orientation.

UT	α (km)	β (km)	pa_α (°)
7.2149	226.5	173.8	193.5
7.5816	227.7	172.9	204.3

riod of 9.40495 h, is shown in Fig. 12 for the epochs of our two observations, along with our convolved and deconvolved images. Although the overall shape of the model appears similar to the images, the model and our images show opposite rotation. The lightcurves of Herculina have been notoriously difficult to interpret (Taylor et al., 1987; Kwiatkowski and Michalowski, 1992; Michalowski et al., 1995), and the inversion model may still be incorrect. For comparison to the biaxial fits, the lightcurve inversion model of $\theta = -60°$ produces clockwise rotation. This comparison of an image or two to model predictions is also how Marchis et al. (2006) resolve some pole ambiguities.

3.1.5. 704 Interamnia

Lightcurves have been obtained from five oppositions, and Michalowski et al. (1995) have used them to derive a shape and an unambiguous pole for Interamnia. They obtain axial ratios of $a/b = 1.11 \pm 0.05$ and $b/c = 1.13 \pm 0.06$, while we obtain $a/b = 1.03 \pm 0.01$ and $b/c = 1.24 \pm 0.10$. Since their $a/c = 1.25 \pm 0.09$ compares better to our $a/c = 1.27 \pm 0.11$, the discrepancy is in the b axis.

A month before we observed this asteroid at Keck Observatory, we observed it at Lick Observatory, and the pole we found at that time was in good agreement with the work of Michalowski et al. (1995). However, our Keck Observatory observations clearly yield a pole at a much higher Ecliptic latitude, although at a similar longitude. Fig. 13 shows the triaxial fit to our Keck Observatory data, Fig. 14 shows the pole locations for the rejected region (our rejected pole is at $[\lambda; \beta] = [306; -35]$), and Fig. 15 shows the accepted region for the pole.[5] The error ellipse around the pole from Michalowski et al. (1995) is drawn in Fig. 15, as well as the wedge error regions around the poles obtained at Lick and Keck Obser-

[5] The two poles from the earlier work of Michalowski (1993) appear to have been inverted by Michalowski et al. (1995). Therefore, in the compilation of poles maintained by Kryszczynska (footnote 3), we have replaced the earlier two poles with the later ones and plotted these in Figs. 14 and 15.

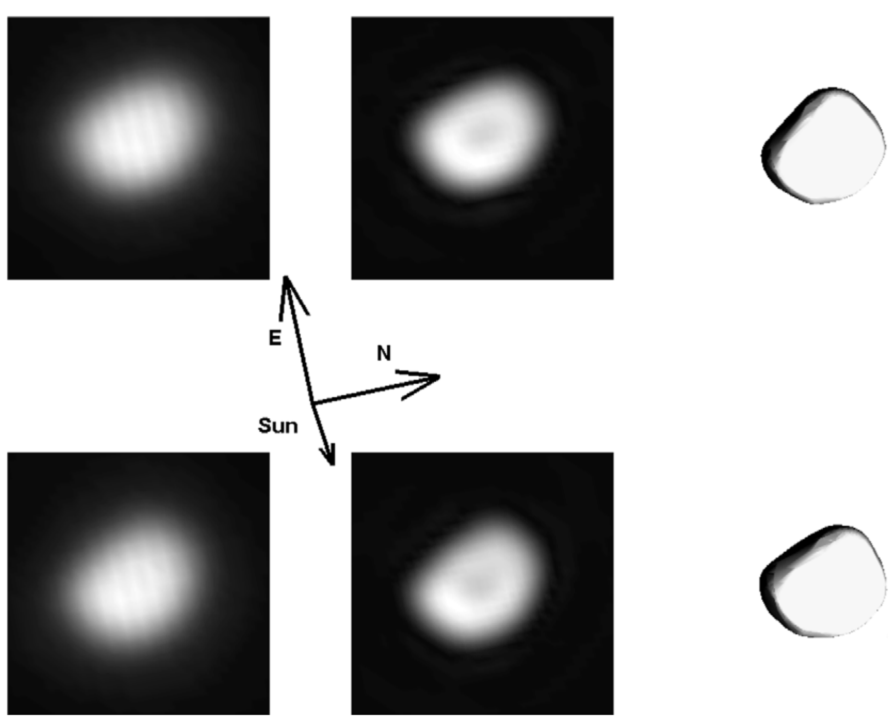

Fig. 12. Convolved (left) and deconvolved (middle) images of Herculina, and lightcurve inversion models at the same rotational phases. The images are 0.3″ (461 km) on a side. It appears that the models are rotating opposite to the images, implying that the model's deep southern hemisphere sub-Earth latitude ($\theta = -60°$) is incorrect. (The dark centers of the deconvolved images are artifacts of the linear deconvolution.)

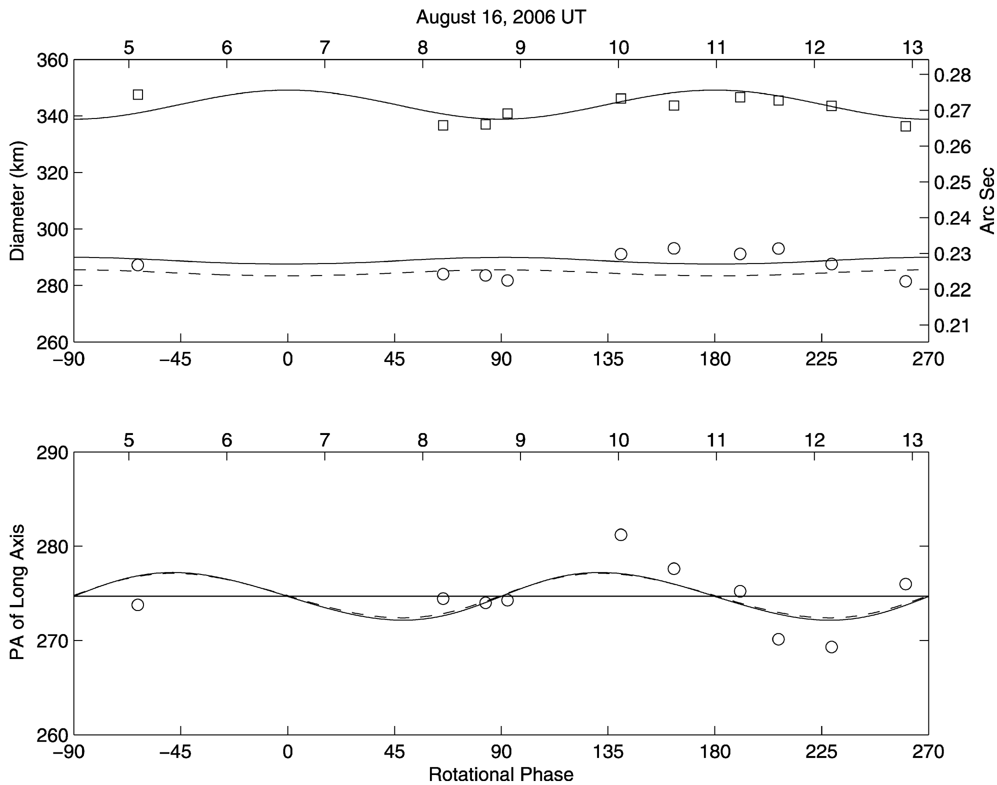

Fig. 13. Triaxial ellipsoid fit for Interamnia. The first point after 5 UT is folded back from the end of the night with the 8.727 h period.

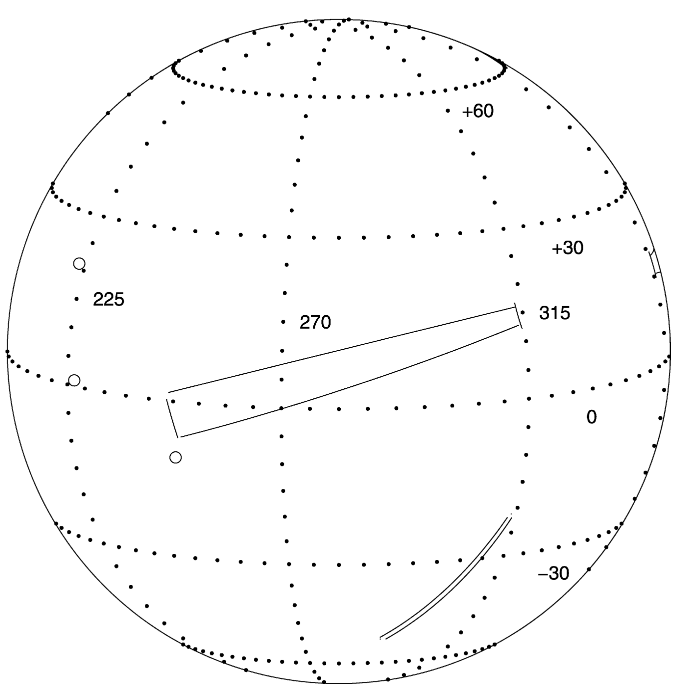

Fig. 14. One set of rotational poles for Interamnia on an Ecliptic globe. This is the rejected region for the pole because the various poles from lightcurve work (3 small circles) do not cluster. The large wedge at center is the uncertainty region around one of the possible poles from the Lick Observatory run in July 2006. At lower right, the smaller uncertainty strip marks one of the poles from our current data from Keck Observatory.

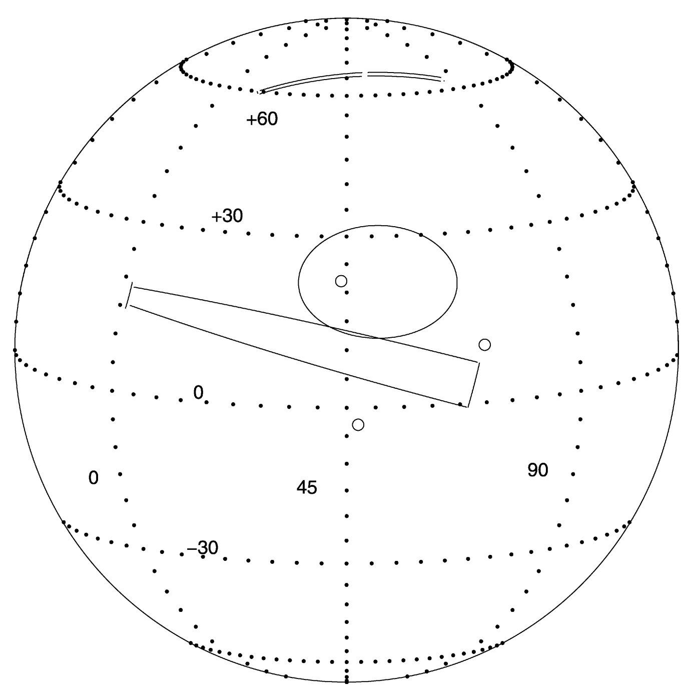

Fig. 15. The other set of rotational poles for Interamnia on an Ecliptic globe. This is the accepted region because the four poles from lightcurves cluster at this longitude. The large circle is the uncertainty region around the pole of Michalowski et al. (1995). The larger wedge is the uncertainty region around the pole we found from a run at Lick Observatory a month earlier, and the much smaller wedge at top is from the current Keck Observatory run.

vatories. While the uncertainty region from our Lick Observatory data is comparable in size to the error area around the pole of Michalowski et al., the uncertainty around our Keck Observatory data is much smaller.

The obliquity between the celestial North Pole and Interamnia's north spin pole is 5.1° for our pole, and 51.7° for the pole of Michalowski et al. (1995). Shifted and added images (5 per epoch) at 9 of the 10 epochs for the Keck Observatory run are shown in

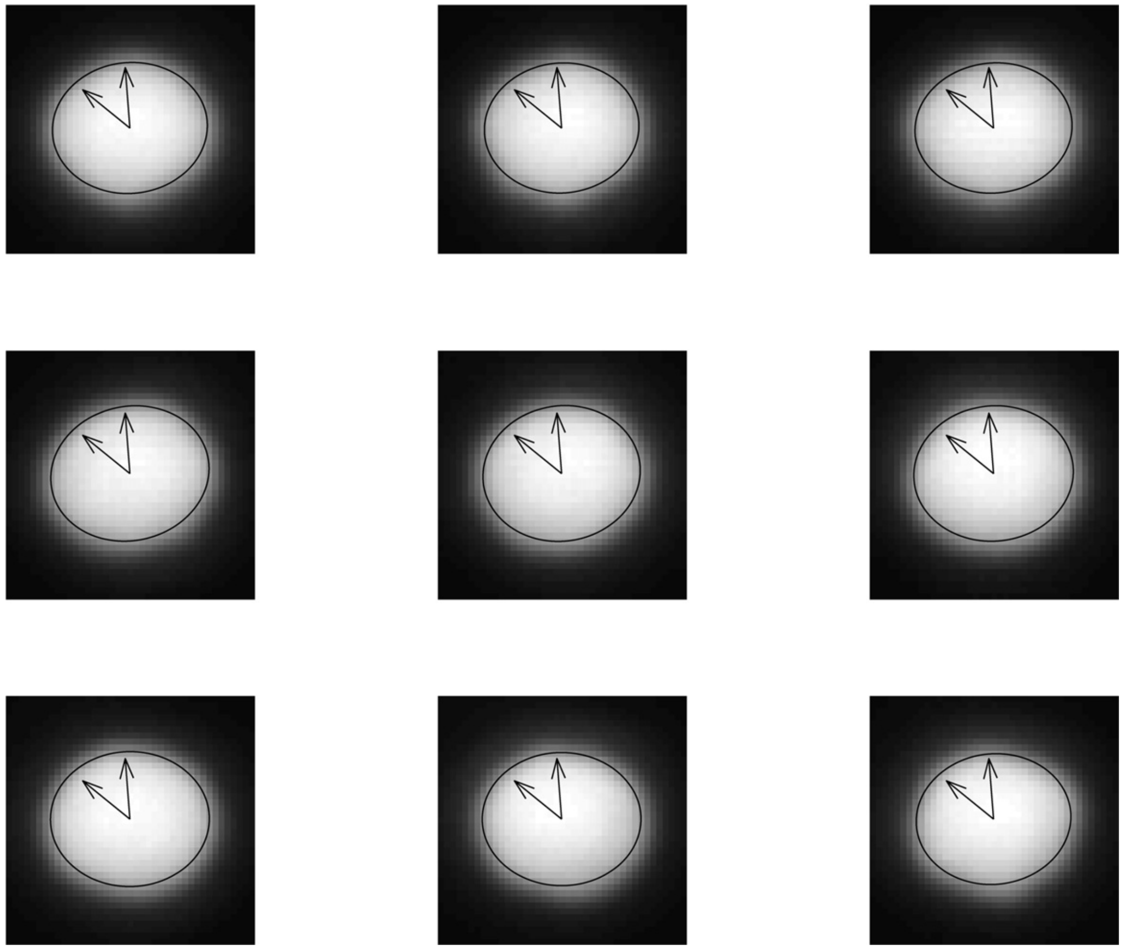

Fig. 16. Centered and added images of Interamnia on August 16, 2006, with the direction to our pole (5° counterclockwise from up—North) and the pole of Michalowski et al. (52° from up) indicated. The ellipse outline of the asteroid as determined from our fit at each epoch is also drawn. The images spill over the edges because of the PSF.

Fig. 16, where celestial North is up, and the direction to both poles are indicated by arrows. The elliptical outline drawn on each image should rock about the line of nodes perpendicular to the direction of the rotational pole. It is obvious that this does not seem to apply for the pole of Michalowski et al. (1995) which is cocked at an angle (obliquity) of 52° from up. Fig. 17 compares selected images to our ellipsoid model and pole, and to the pole and (assumed) ellipsoid model of Michalowski et al. (1995). Again, the images do not seem to corroborate the latter's pole.

Of all the asteroid's studied with AO at Lick and Keck Observatories, and compared to the results of lightcurve work, Interamnia from Keck Observatory shows the greatest and clearest discrepancy in pole location. It might be easy to dismiss our Keck Observatory pole as anomalous, but the images clearly indicate a pole with small obliquity. On the other hand, there is nothing to indicate that the Michalowski et al. result for Interamnia is suspect. One possible solution is that Interamnia is precessing, which would lead to large uncertainties for the pole solution from lightcurves gathered over long periods of time, and would also lead to different pole solutions obtained on different nights with our technique.

4. Search for satellites

As a secondary project, the area around every image of each asteroid was searched for satellites, but, with one exception, not even stars were detected around any asteroid. Three stars were found that trailed past Herculina even while dithering across the five-spot pattern, two in the first observation only, and the third star in both observations. The five-spot pattern allows a search around the asteroid out to three-quarters of the field, 7.5″ or at the distance of Herculina, around 11,500 km. The stars were quite faint and only the results (not images) of measuring the separation and distance from Herculina at the center are shown, as Fig. 18. The brightness of Herculina is found from $\pi I\alpha\beta$, where the parameters are determined in the Fourier plane with the PBD method of Section 2, I being the mean intensity across the face of the asteroid, and the brightness of the stars are found from a Gaussian fit of a small sub region containing the stars. Two images of stars fell on the edge of a frame and were not fit nor used to find the brightness of the stars. Thus the brightness ratio, or Δ_m, of star A was determined from all 3 frames where it was observed, to be 8.1 ± 0.1, 2 of 3 frames were used for star B ($\Delta_m = 8.9 \pm 0.3$), and 5 of 6 were used for star C (7.5 ± 0.1).

Using the search square radius of $7.5'' = 11{,}515$ km, we conclude that within 11,500 km of the asteroid no satellite exists around Herculina down to 8.9 magnitudes fainter. Using Herculina's mean diameter of 200 km from Table 7, and assuming that a satellite would have the same albedo as the asteroid, any such satellite must be smaller than 3.3 km. For the other asteroids, we can also conclude that no satellite exists down to 8.9 magnitudes fainter than the primary. (For a more deliberate effort to detect satellites around asteroids see Marchis et al., 2006.)

5. Summary

Short of a visit by spacecraft, or of radar imaging of near-Earth asteroids, large telescope AO images will be the best way to study

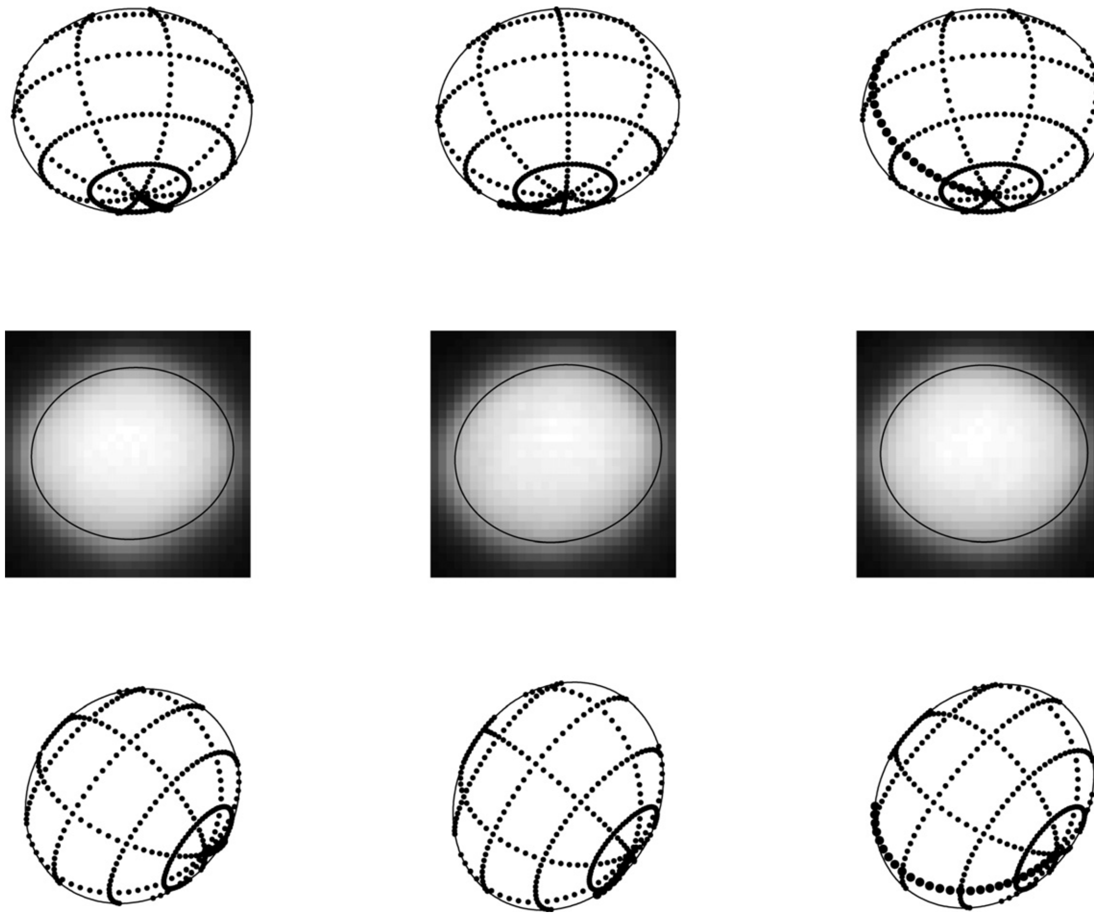

Fig. 17. Comparison of our model and orientation (top) to our images of Interamnia, and to the predicted model and orientation from Michalowski et al. (bottom). The second, fifth, and eighth epochs from Fig. 12 are compared. The biggest difference between the orientation of the image and our model occurs for the middle image, as can be also seen in Fig. 12 at 10 UT in the lower sub-plot. The heavier dotted meridians are where the asterocentric longitude is 0° and pass over the tip of the long axis, *a*. The sub-Earth latitude for our model is $\theta = -26°$ and $\theta = -19°$ for the Michalowski et al. pole.

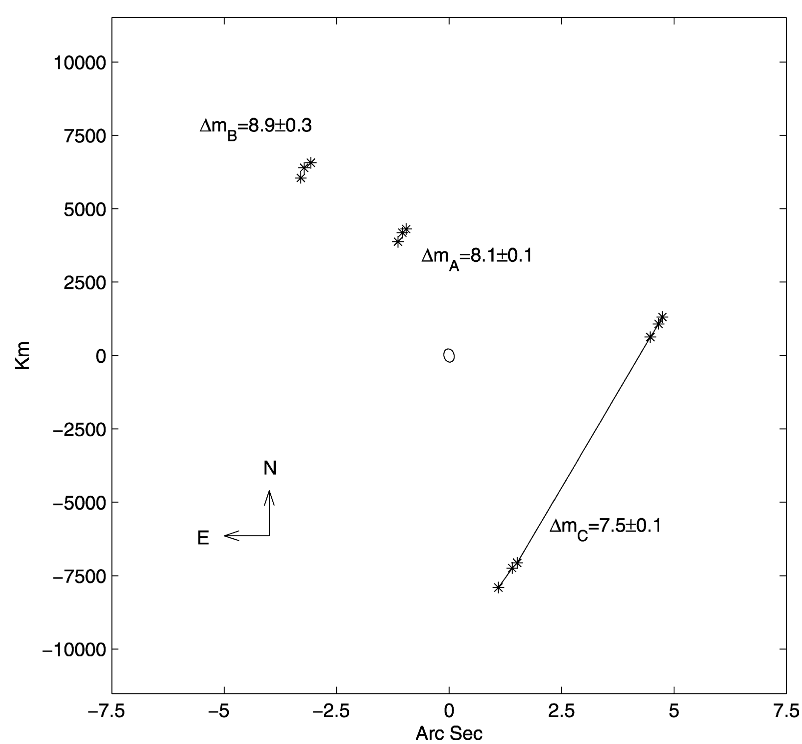

Fig. 18. Positions of three stars with respect to Herculina. The apparent direction of the stars is NW. Herculina, in the center, is drawn to scale.

resolved asteroids, and making the triaxial ellipsoid assumption continues to be a useful tool to derive an asteroid's dimensions and spin pole direction over a few rotations. Further refinements can then be made on observed departures from the triaxial ellipsoid assumptions.

Pallas' pole is resolved from our Lick and Keck Observatory observations a month apart, and agrees with a growing consensus. Its dimensions are determined to better than 1% in its equatorial plane and to 3% for its short axis. However, a comparison to its two well observed occultations reveals systematic differences in its appearance. Antigone's a and b dimensions are found to within 2.5%, but its c dimension to only 15%. Its pole ambiguity is resolved by appealing to lightcurves. The agreement between our images of Antigone and the LCI model (footnote 2) of Torppa et al. (2003) is excellent. Aspasia's dimensions are determined to better than 2.5%, but only by assuming $b = c$, and its overall size of $\bar{d} = 180 \pm 2$ differs the most from the IRAS results of 162 ± 7 km. Its pole ambiguity is resolved with help from the work of Blanco and Riccioli (1998).

The biggest discrepancy occurs for the location of the pole for Interamnia, which differs even from our own results from Lick Observatory a month earlier. This asteroid deserves more study, because if the pole discrepancy stands up, it may suggest that Interamnia is precessing. The other discrepant result is that we find Herculina to rotate counterclockwise (north to east), whereas the LCI model (footnote 2) of Kaasalainen et al. (2002) predicts clockwise rotation for our observations.

No satellites were detected around any of the asteroids. Three stars seen drifting past Herculina set a lower limit of 8.9 magnitudes for a primary to satellite brightness ratio.

Acknowledgments

Observational and travel support for Drummond was provided by the Directed Energy Directorate of the Air Force Research Laboratory, with a special thanks to LtCol Dennis Montera. We appreciate the detailed comments provided by Peter Thomas and an anonymous referee. The authors also wish to recognize and acknowledge the very significant cultural role and reverence that the summit of Mauna Kea has always had within the indigenous Hawaiian community. We are most fortunate to have the opportunity to conduct observations from this mountain top. This research made use of NASA's Astrophysics Data System and of JPL's Horizons On-Line Ephemeris System.

References

Blanco, C., Riccioli, D., 1998. Pole coordinates and shape of 30 asteroids. Astron. Astrophys. Suppl. Ser. 131, 385–394.

Carry, B., Dumas, C., Fulchignoni, M., Merline, W.J., Berthier, J., Hestroffer, D., Fusco, T., Tamblyn, P., 2008. Near-infrared mapping and physical properties of the dwarf-planet Ceres. Astron. Astrophys. 478, 235–244.

Carry, B., Dumas, C., Kaasalainen, M., Berthier, J., Merline, W.J., Erard, S., Conrad, A., Drummond, J.D., Hestroffer, D., Fulchignoni, M., Fusco, T., 2009. Physical properties of 2 Pallas. Icarus, in press.

Christou, J.C., Drummond, J.D., 2006. Measurements of binary stars, including two new discoveries, with the Lick Observatory adaptive optics system. Astron. J. 131, 3100–3108.

Conrad, A.R., Dumas, C., Merline, W.J., Drummond, J.D., Campbell, R.D., Goodrich, R.W., Le Mignant, D., Chaffee, F.H., Fusco, T., Kwok, S.A., Knight, R.I., 2006. Direct measurement of the size, shape, and pole of 511 Davida with Keck AO in a single night. Icarus 191, 616–627.

Conrad, A.R., Merline, W.J., Drummond, J.D., Tamblyn, P.M., Dumas, C., Carry, B., Campbell, R.D., Goodrich, R.W., Owen, W.M., Chapman, C.R., 2008a. S/2008 (41) 1. IAU Circular 8930, 31 March, 2008.

Conrad, A., Carry, B., Drummond, J.D., Merline, W.J., Dumas, C., Owen, W.M., Chapman, C.R., Tamblyn, P.M., Goodrich, R.W., Campbell, R.D., 2008b. Shape and size of Asteroid (41) Daphne from AO imaging. Bull. Am. Astron. Soc. 40, 346. #28.12.

Descamps, P., and 18 colleagues, 2008. New determination of the size and bulk density of the binary Asteroid 22 Kalliope from observations of mutual eclipses. Icarus 196, 578–600.

Drummond, J.D., 1998. Adaptive optics Lorentzian point spread function. In: Bonaccini, D., Tyson, R.K. (Eds.), Adaptive Optical System Technologies. In: Proc. SPIE, vol. 3353. SPIE, Bellingham, WA, pp. 1030–1037.

Drummond, J.D., 2000. Measuring asteroids with adaptive optics. In: Ageorges, N., Dainty, C. (Eds.), Laser Guide Star Adaptive Optics for Astronomy. Kluwer Academic Publishers, Dordrecht, pp. 243–262.

Drummond, J., Christou, J., 2008. Triaxial ellipsoid dimensions and rotational poles of seven asteroids from Lick Observatory adaptive optics images, and of Ceres. Icarus 197, 480–496.

Drummond, J.D., Cocke, W.J., Hege, E.K., Strittmatter, P.A., Lambert, J.V., 1985. Speckle interferometry of asteroids. I. 433 Eros. Icarus 61, 132–151.

Dunham, D.W., Herald, D., 2008. Asteroid Occultations V6.0. EAR-A-3-RDR-OCCULTATIONS-V6.0. NASA Planetary Data System.

Dunham, D.W., and 45 colleagues, 1990. The size and shape of (2) Pallas from the 1983 occultation of 1 Vulpeculae. Astron. J. 99, 1636–1662.

Kaasalainen, M., Torppa, J., 2001. Optimization methods for asteroid lightcurve inversion. I. Shape determination. Icarus 153, 24–36.

Kaasalainen, M., Torppa, J., Muinonen, K., 2001. Optimization methods for asteroid lightcurve inversion. II. The complete inverse problem. Icarus 153, 37–51.

Kaasalainen, M., Torppa, J., Piironen, J., 2002. Models of twenty asteroids from photometric data. Icarus 159, 369–395.

Kryszczyńska, A., La Spina, A., Paolicchi, P., Harris, A.W., Breiter, S., Pravec, P., 2007. New findings on asteroid spin–vector distributions. Icarus 192, 223–237.

Kwiatkowski, T., Michalowski, T., 1992. Spin vector and shape of 532 Herculina. In: Asteroids Comets Meteors 1991, pp. 333–336.

Magnusson, P., 1989. Pole determination of asteroids. In: Binzel, P.B., Gehrels, T., Matthews, M.S. (Eds.), Asteroids II. Univ. of Arizona Press, Tucson, pp. 1180–1190.

Marchis, F., Hestroffer, D., Descamps, P., Berthier, J., Laver, C., de Pater, I., 2005. Mass and density of Asteroid 121 Hermione from an analysis of its companion orbit. Icarus 178, 450–464.

Marchis, F., Kaasalainen, M., Hom, E.F.Y., Berthier, J., Enriquez, J., Hestroffer, D., Le Mignant, D., de Pater, I., 2006. Shape, size and multiplicity of main-belt asteroids. I. Keck adaptive optics survey. Icarus 185, 39–63.

Merline, W.J., Conrad, A.R., Drummond, J.D., Carry, B., Dumas, C., Tamblyn, P.M., Chapman, C.R., Owen, W.M., Durda, D.D., Campbell, R.D., Goodrich, R.W., 2008. Discovery of an extreme mass-ratio satellite of (41) Daphne in a close orbit. In: Asteroids, Comets, Meteors 2008, held July 14–18, 2008 in Baltimore, MD. LPI Contribution No. 1405.

Michalowski, T., 1993. Poles, shapes, senses of rotation, and sidereal periods of asteroids. Icarus 106, 563–572.

Michalowski, T., Velichko, F.P., di Martino, M., Krugly, Y.N., Kalashnikov, V.G., Shevchenko, V.G., Birch, P.V., Sears, W.D., Denchev, P., Kwiatkowski, T., 1995. Models of four asteroids: 17 Thetis, 52 Europa, 532 Herculina, and 704 Interamnia. Icarus 118, 292–301.

Taylor, R.C., Birch, P.V., Drummond, J., Pospieszalska-Surdej, A., Surdej, J., 1987. Asteroid 532 Herculina—Lightcures, pole orientation and a model. Icarus 69, 354–369.

Tedesco, E.F., Veeder, G.J., Fowler, J.W., Chillemi, J.R., 1992. The IRAS Minor Planet Survey—Final Report (PL-TR-92-2049). Phillips Laboratory, Hanscom Air Force Base, MA.

Torppa, J., Kaasalainen, M., Michalowski, T., Kwiatkowski, T., Kryszczyńska, A., Denchev, P., Kowalski, R., 2003. Shapes and rotational properties of thirty asteroids from photometric data. Icarus 164, 346–383.

Wasserman, L.H., and 17 colleagues, 1979. The diameter of Pallas from its occultation of SAO 85009. Astron. J. 84, 259–268.